NUCLEAR THEORY, Vol. 35 (2016)
eds. M. Gaidarov, N. Minkov, Heron Press, Sofia

Study of Alternating-Parity Spectra in Ba-Ce Nuclei

N. Minkov, **S. Drenska**, **P. Yotov**

Institute of Nuclear Research and Nuclear Energy, Bulgarian Academy of Sciences, 72 Tzarigrad Road Blvd., BG-1784 Sofia, Bulgaria

Abstract. We study the specific features of alternating-parity spectra in the region of Ba and Ce nuclei in comparison to the structure of analogous excitations in actinide nuclei. The spectra in Ba-Ce nuclei are characterized by larger parity-shift at low angular momenta, compared to Ra and Th nuclei, which sharply decreases at the higher levels forming a single band with irregular-staggering structure. In addition, our analysis shows that the structure of the even-parity level-sequences strongly deviates from the pure rotation behaviour, whereas the odd-parity sequences exhibit rather well pronounced rotation structure. Given the above peculiarities of the considered spectra we examine the possibility to describe them within the framework of the Quadrupole-Octupole Rotation Model (QORM) earlier developed in Sofia group. The preliminary results obtained for the alternating-parity spectra of ^{144,146}Ba and ^{144,146,148,150}Ce support the applicability of the model in this region.

1 Introduction

The observation of alternating-parity (AP) bands in even-even nuclei and quasi parity-doublet spectra in odd-mass nuclei attended by electric E1 and E3 γ-transitions is quite unambiguously associated with the manifestation of reflection-asymmetric deformations [1, 2]. Although the concept for explaining these phenomena was extensively developed on the basis of nuclear quadrupole-octupole (QO) shapes, the question about the stability of such a shape in the ground and the excited states remains open. The reason is that one never observes neither ideal octupole (or AP) bands nor parity-doublets. From theoretical point of view the challenge is to elaborate a model scheme capable to explore the limits in which the octupole (reflection-asymmetric) shape manifest as a stable deformation mode or only softly influences the collective motion of the nucleus. In our previous works we developed a model approach aiming to study the evolution of QO collectivity both, along the variety of nuclei exhibiting such a behaviour and with the increasing of the angular momentum in a particular spectrum [3–9]. In the limit of stable QO deformations the formalism involves the so-called Quadrupole-Octupole Rotation Model (QORM) combined with pure octupole vibrations [3, 4]. In [4] it was tested on several octupole bands in the light actinide nuclei Ra and Th, whereas its capability in the region of Ba and Ce

nuclei, where such bands also exist, is not yet checked. In the cases of soft QO-deformation degrees of freedom (rare-earth nuclei, heavy actinides, odd-mass nuclei) the approach assumes the so-called Coherent Quadrupole-Octupole Motion (CQOM) [5,6]. It involves mixed QO vibrations and rotations and describes the structure of both, yrast and non-yrast QO spectra in even-even and odd-mass nuclei [7, 8].

In the last few years two experimental works reporting the observation (or more precisely, the reconfirmation) of stable octupole deformation in the ground states of ^{224}Ra [10] and ^{144}Ba [11] inspired a new activity on the subject. Partially motivated by this fresh impulse in the area and also realizing the need to validate our model formalism in the region of Ba-Ce nuclei, in the present article we examine the structure of octupole spectra in this region and show preliminary results of the QORM application to the AP bands in ^{144,146}Ba and ^{144,146,148,150}Ce. As it will be seen below, the obtained results give us further motivation to implement a more detailed model study of the spectra not only in this region but also in the previously explored region of light actinide nuclei, by including into description the related electric transition probabilities.

The paper is organized as follows. In Section 2 the specific structure of the spectrum in Ba-Ce nuclei is discussed. In Section 3 the QORM formalism is briefly recalled. In Section 4 the results of the model descriptions are given with an attending discussion. In Section 5 concluding remarks are given.

2 Features of Alternating-Parity Spectra in Ba-Ce Nuclei

First we recall that the Ba and Ce nuclei are recognized as a region in which the appearance of octupole deformation is favoured on the basis of the shell model estimations [2]. In this model there are several particle-filling numbers, for which orbitals with opposite parity (e.g. from neighbouring shells) and orbital-momentum difference $\Delta l = 3$ may couple near the Fermi level, namely **34** ($g_{\frac{9}{2}} \otimes p_{\frac{3}{2}}$), **56** ($h_{\frac{11}{2}} \otimes d_{\frac{5}{2}}$), **88** ($i_{\frac{13}{2}} \otimes f_{\frac{7}{2}}$), **134** ($j_{\frac{15}{2}} \otimes g_{\frac{9}{2}}$), and which favour the appearance of strong octupole correlations/deformation in the respective nuclei.

Thus, in Ba isotopes we have the octupole "magic number" Z=56 and, moreover, in ^{144}Ba another one, $N = 88$, appear. Ce isotopes, with Z=58, are situated in the close vicinity and in addition ^{146}Ce has $N = 88$. In a similar way one may also expect octupole correlations in some Xe (Z=54) isotopes, with ^{142}Xe having $N = 88$. For comparison, in the light actinide nuclei one has: Z=88 in Ra isotopes, with ^{222}Ra having also $N = 134$; neighbouring $Z = 86$ in Rn isotopes, with ^{220}Rn having $N = 134$; and $Z = 90$ in Th isotopes, with ^{224}Th having $N = 134$. Of course, these estimations are rather rough since in the conditions of pronounced deformation the shell structure and the orbital couplings may not follow exactly the above "magic filling". Nevertheless, the experimental data indeed reveal the presence of bands that can be identified as based on octupole degrees of freedom, especially in the nuclei $^{140-148}$Ba, ^{144,146}Ce, $^{148-152}$Ce (though in the last 3 nuclei the negative-parity sequence starts from angular mo-

mentum $I = 7^-$) and in ^{140,142}Xe [12]. In all these nuclei one can observe AP structure of the yrast spectrum with the usual displacement at the beginning of the negative-parity sequence above the positive-parity one.

To estimate the specific structure of these spectra we performed a separate fit of the positive- and negative-parity levels in each spectrum through the following simple parabolic expression

$$E(I^\pi) = \Delta E^- + A_\pi\, I^\pi(I^\pi + \omega_\pi), \qquad \pi = (\pm), \tag{1}$$

where ΔE^- measures the initial shift up of the negative-parity levels, A_π are separate inertia parameters for both sequences and ω_π are respective parameters of deviation from the pure rotation structure.

The result of the fits is shown in Table 1. It is seen that the root-mean square (rms) deviation between the interpolated and experimental energy values vary for the different nuclei in the range 15–60 keV. The following differences between the parameters values obtained for the Ba-Ce isotopes and those for the nuclei ^{224}Ra and ^{224}Th (considered for comparison) should be remarked:

i) The parity shift ΔE^- in the beginning of Ba-Ce spectra is much larger compared to that in Ra-Th.

ii) In most of Ba-Ce nuclei the values of the deviation parameter ω_+ are much larger than those of ω_-, whereas in Ra-Th these two quantities do not differ considerably. An exception is observed in ^{148}Ce and ^{150}Ce which can be referred to the nuclei with pronounced QO softness, as shown in sec. 4.

Further we analyse the fine structure of AP bands through the following high-order $\Delta I = 1$ staggering quantity

$$\mathrm{Stg}(I) = 6\Delta E(I) - 4\Delta E(I-1) - 4\Delta E(I+1) + \Delta E(I+2) + \Delta E(I-2)\,, \tag{2}$$

Table 1. Parameters of parabolic fits (by Eq. (1)) of the yrast positive- and negative-parity levels in several Ba-Ce isotopes and the nuclei ^{224}Ra and ^{224}Th. See the text for explanation of the parameters.

Nucl	ΔE^- [keV]	A_+ [keV]	A_- [keV]	ω_+	ω_-	rms [keV]
^{224}Ra	64	4.0	4.3	17.3	14.2	51.07
^{224}Th	141	4.0	4.2	14.2	11.0	41.81
^{142}Ba	1105	10.2	11.2	18.3	0.7	45.56
^{144}Ba	701	8.8	11.4	12.8	1.4	34.95
^{146}Ba	710	7.1	12.7	17.8	0.2	58.09
^{148}Ba	675	10.2	12.2	7.1	-0.2	21.47
^{144}Ce	1029	15.0	18	11.9	0.74	21.48
^{146}Ce	843	11.2	12.3	11.1	1.3	33.74
^{148}Ce	319	5.65	6.7	21.5	15.0	61.19
^{150}Ce	551	8.0	7.0	7.5	9.9	33.30
^{152}Ce	810	9.8	9.2	3.3	0.1	14.70

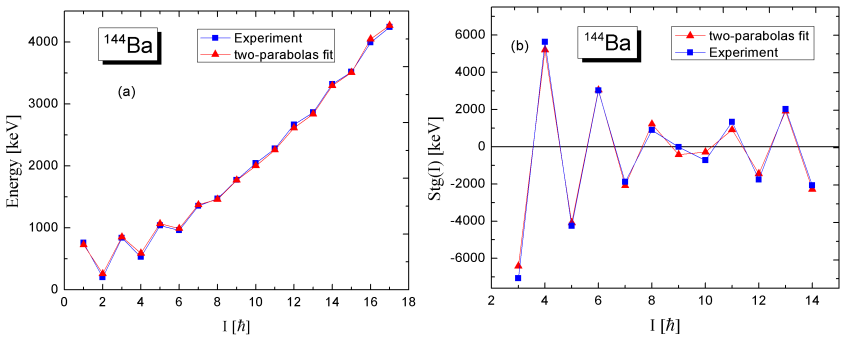

Figure 1. AP levels (a) and $\Delta I = 1$ staggering pattern (b) for ^{144}Ba from the 2-parabolas fit (Eq. (1)) and experimental data [12]. Parameters of the fit are given in Table 1.

where $\Delta E(I) = E(I+1) - E(I)$. In Figure 1 we show the fitted and the experimental levels of ^{144}Ba together with the respective $\Delta I = 1$ staggering patterns. We see that the experimental staggering (reproduced by the fit) is quite large in the beginning, then sharply decreases and after undergoing a "beating" between $I = 8$ and 10 reappears at higher I. The illustrated reproduction of the octupole-band structure in ^{144}Ba as well as the reasonable rms values given in Table 1 suggests that the parameters of the two-polynomial fits can be used as empirical characteristics of the observed AP bands and relevant measures for their deviation from the pure rotation structure. Providing this remark we can conclude that the spectra of Ba-Ce isotopes exhibit a rather strongly perturbed rotation dynamics. Therefore, it is indeed interesting to see (in Section 4) to what extent these spectra can be described within the QORM framework.

3 Octupole Oscillations and Quadrupole-Octupole Rotation Mode

In the QORM approach it is assumed that at low angular momenta the nucleus is characterized by a soft octupole shape superposed on the top of a stable quadrupole deformation, while with the increasing spin the total QO shape is stabilized [4]. Then it is considered that at low spin the system is capable to perform octupole oscillations determined by a Hamiltonian including symmetric angular-momentum-dependent double-well potential in the axial octupole deformation variable β_3 [4]

$$H_{\rm osc}^{\rm oct} = -\frac{\hbar^2}{2B_3}\frac{d^2}{d\beta_3^2} + \frac{1}{2}C_3{\beta_3}^2 + \frac{I(I+1)}{2(d_2+d_3\beta_3^2)}, \qquad (3)$$

where B_3 and C_3 are octupole mass and stiffness parameters, while d_2 and d_3 are rigid-quadrupole and soft-octupole inertia parameters, respectively. The parameter C_3 is determined by fixing the minimum of the potential term in (3) at given octupole deformation value $\beta_{3\,\rm min}$. In addition the potential term is rede-

termined with respect to a zero-energy minimum, bringing (3) to [4]

$$\tilde{H}^{\rm oct}_{\rm osc} = -\frac{\hbar^2}{2B_3}\frac{d^2}{d\beta_3^2} + \frac{I(I+1)d_3^2(\beta_3^2-\beta_{3\rm min}^2)^2}{2(d_2+d_3\beta_{3\rm min}^2)^2(d_2+d_3\beta_3^2)}. \qquad (4)$$

The numerical solution of the Schrödinger equation for Hamiltonian (4) at given I determines the energy shift $\delta E_{\rm osc}(I) = E^{(-)}_{\rm osc}(I) - E^{(+)}_{\rm osc}(I)$ between the opposite-parity states in the octupole band and subsequently the octupole-vibration contribution to the collective energy

$$E_{\rm osc}(I) = E_0 - \frac{1}{2}(-1)^I \delta E_{\rm osc}(I), \qquad (5)$$

where E_0 is a constant which determines the origin of the energy scale. Being strong at low I the parity-shift rapidly decreases, together with the reduction of the octupole-vibration mode, as a result of the increase of the potential barrier with the increasing I. This is shown in Figures 1 and 3 in [4] (see also Figure 1 in [9]).

At the higher I the octupole deformation is stabilized and the nucleus performs a rotation motion governed by the complex deformed shape. This motion is described by the point-symmetry based QORM Hamiltonian [3]

$$\hat{H}_{\rm QORM} = \hat{H}_{\rm quad} + \hat{H}_{\rm oct} + \hat{H}_{\rm qoc}\ . \qquad (6)$$

It includes the following quadrupole and octupole rotation terms

$$\hat{H}_{\rm quad} = A\hat{I}^2 + A'\hat{I}_z^2, \qquad \hat{H}_{\rm oct} = \hat{H}_{A_2} + \sum_{r=1}^{2}\sum_{i=1}^{3}\hat{H}_{F_r(i)}. \qquad (7)$$

The octupole part $\hat{H}_{\rm oct}$ is constructed through the irreducible representations A_2, $F_1(i)$ and $F_2(i)$ ($i = 1, 2, 3$) of the octahedron (O) point–symmetry group, which correspond to different octupole shapes. Here

$$\hat{H}_{A_2} = a_2\frac{1}{4}[(\hat{I}_x\hat{I}_y + \hat{I}_y\hat{I}_x)\hat{I}_z + \hat{I}_z(\hat{I}_x\hat{I}_y + \hat{I}_y\hat{I}_x)]\ , \qquad (8)$$

$$\begin{aligned}
\hat{H}_{F_1(1)} &= \frac{1}{2}f_{11}(5\hat{I}_z^3 - 3\hat{I}_z\hat{I}^2) \qquad & \hat{H}_{F_2(1)} &= f_{21}\frac{1}{2}[\hat{I}_z(\hat{I}_x^2 - \hat{I}_y^2) + (\hat{I}_x^2 - \hat{I}_y^2)\hat{I}_z] \\
\hat{H}_{F_1(2)} &= \frac{1}{2}f_{12}(5\hat{I}_x^3 - 3\hat{I}_x\hat{I}^2) \qquad & \hat{H}_{F_2(2)} &= f_{22}(\hat{I}_x\hat{I}^2 - \hat{I}_x^3 - \hat{I}_x\hat{I}_z^2 - \hat{I}_z^2\hat{I}_x) \\
\hat{H}_{F_1(3)} &= \frac{1}{2}f_{13}(5\hat{I}_y^3 - 3\hat{I}_y\hat{I}^2) \qquad & \hat{H}_{F_2(3)} &= f_{23}(\hat{I}_y\hat{I}_z^2 + \hat{I}_z^2\hat{I}_y + \hat{I}_y^3 - \hat{I}_y\hat{I}^2)\ ,
\end{aligned} \qquad (9)$$

where a_2 and $f_{r\,i}$ ($r = 1, 2$; $i = 1, 2, 3$) are model parameters, whereas $\hat{I}_k$ ($k = x, y, z$) are the projections of the operator $\hat{I}$ on the intrinsic-frame axes. The last term in (6) represents a higher-order QO interaction [3]

$$\hat{H}_{\rm qoc} = f_{\rm qoc}\frac{1}{I^2}(15\hat{I}_z^5 - 14\hat{I}_z^3\hat{I}^2 + 3\hat{I}_z\hat{I}^4). \qquad (10)$$

The energy corresponding to the diagonal part of $\hat{H}_{\rm QORM}$ in the axial-rotor states $|IK\rangle$ with angular momentum I and projection K on the z-axis has the form

$$\begin{aligned} E_K(I) &= AI(I+1) + A'K^2 + \frac{1}{2}f_{11}\left[5K^3 - 3KI(I+1)\right] \\ &+ f_{\rm qoc}\frac{1}{I^2}\left[15K^5 - 14K^3I(I+1) + 3KI^2(I+1)^2\right] \ . \end{aligned} \quad (11)$$

The QORM spectrum is obtained by diagonalizing the Hamiltonian (6) for given I in the basis $|IK\rangle$ and selection of the eigenvalue which corresponds to the minimum of the energy as a function of the leading K-value. It was found that the leading K-values in the minima increase by a unit after any two units of increasing I with some exceptions where K is changed at both subsequent I-values. This structure of the QORM energy levels corresponds to the "beat" staggering patterns observed in the high-spin regions of octupole spectra.

By combining the solutions of the octupole-vibration Hamiltonian (4) with those of QORM (6) one gets the complete model structure of an AP band. In [4] we have applied this formalism to describe the AP bands together with the beat staggering patterns in Ra and Th isotopes.

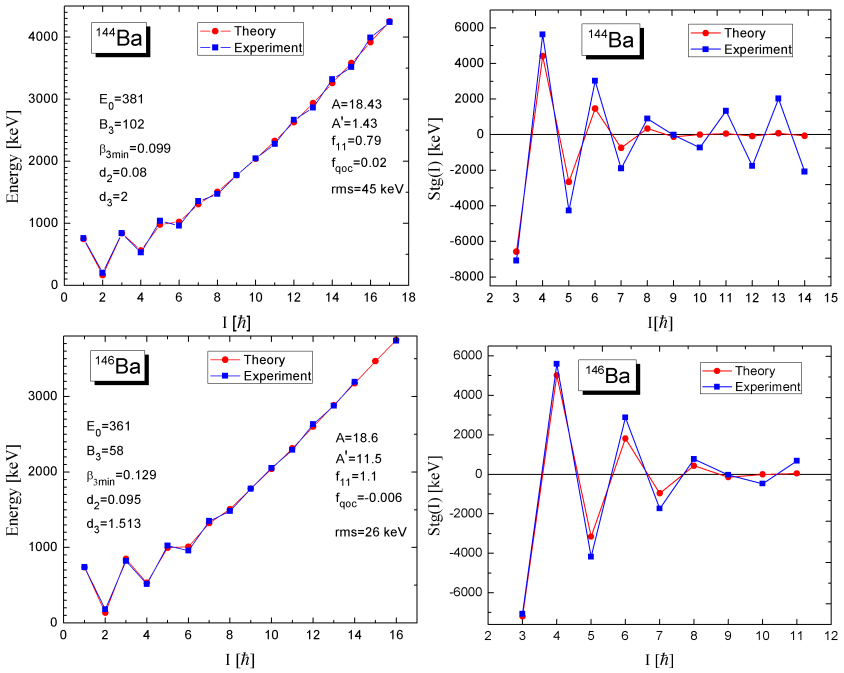

Figure 2. Theoretical and experimental AP levels (left panels) and $\Delta I = 1$ staggering patterns (right panels) for ^{144}Ba and ^{146}Ba. The parameters B_3 and d_2,d_3 are given in $\hbar^2$/MeV and MeV^{-1}, respectively, $\beta_{3\rm min}$ is dimensionless, while the other parameters are in keV. Data from [12].

4 Numerical Results and Discussion

We have applied the model formalism of sec. 3 to the AP bands of the nuclei ^{144,146}Ba and ^{144,146,148,150}Ce. The model parameters were adjusted to experimental data [12]. In Tables 2 and 3 the obtained theoretical energy levels are compared with the corresponding experimental data. A number of missing experimental levels are predicted. In Figures 2–4 this comparison is given graphically and in addition the respective theoretical and experimental $\Delta I = 1$ staggering patterns are compared. Also, the parameters values are given there.

The general observation is that the QORM formalism reproduces reasonably good the structure of the octupole spectra in the considered nuclei with energy rms deviations between 23 and 45 keV. This is a bit not too good compared to the result obtained in [4] for the nuclei ^{224,226}Ra and ^{224,226}Th, where the rms factor vary between 8 and 20 keV. Actually the present result is not unexpected and indeed reflects the conclusions reached in the analysis of Section 2. Comparing the staggering patterns given in Figures 2–4 for the Ba-Ce nuclei with those for Ra-Th (Figures 4–7 in [4]) we see the much larger (by a factor of 2-3) parity-shift effect in the beginning of the Ba-Ce spectra. This is also indicated by the values of the parameter ΔE^- in Table 1. Regarding the two nuclei ^{144}Ba

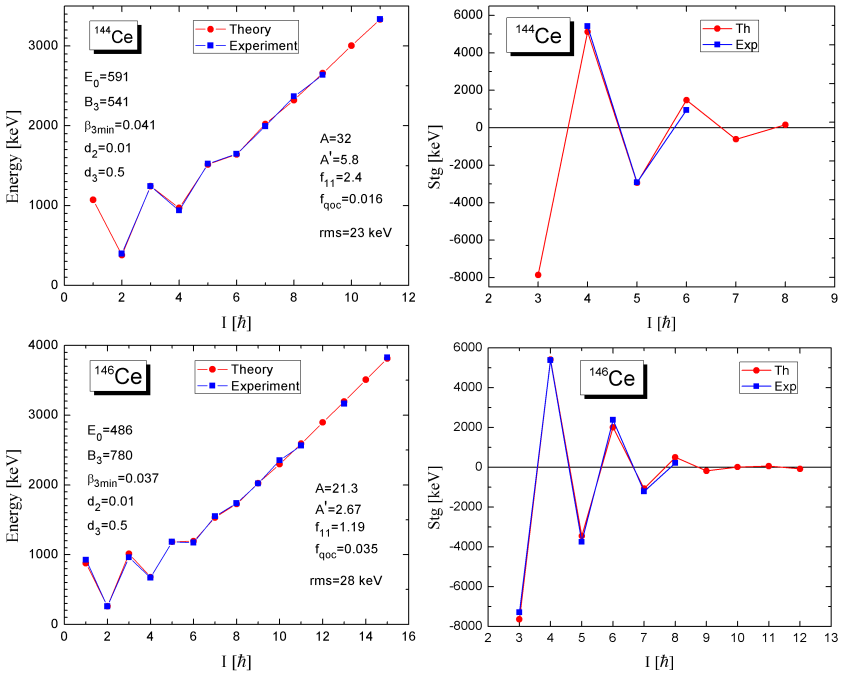

Figure 3. The same as Figure 2, but for ^{144}Ce and ^{146}Ce.

Table 2. Theoretical and experimental energy levels (in keV) of the AP bands in ^{144}Ba, ^{146}Ba, ^{144}Ce and ^{146}Ce. The respective parameters values are given in Figures 2 and 3. The rms deviations (in keV) are given at the bottom. Data from [12].

	^{144}Ba		^{146}Ba		^{144}Ce		^{146}Ce	
I	Th	Exp	Th	Exp	Th	Exp	Th	Exp
1	749.1	758.9	735.5	738.8	1072.0		877.9	924.6
2	165	199.3	134.6	181.1	378.2	397.4	258.9	258.5
3	839.5	838.4	847.3	821	1242.6	1242.2	1011.9	960.7
4	561.9	530.2	531.6	513.5	969.1	938.7	677.2	668.4
5	980.4	1038.8	996.4	1024.4	1516.1	1523.7	1182.3	1183.0
6	1022.2	961.5	1010.1	958.2	1640.6	1646.8	1192.9	1171.3
7	1309.8	1355.2	1321.9	1349	2022.6	1994.3	1532.6	1551.1
8	1505.8	1470.8	1506.9	1482.4	2322.0	2368.8	1728.1	1736.8
9	1775	1773.0	1780.1	1777.5	2659.3	2636.7	2021.8	2019.4
10	2041.2	2044.3	2041	2051.8	3003.7		2298.1	2351.5
11	2325.9	2279.1	2313.1	2292.5	3333.8	3335.7	2589.2	2562.7
12	2630.2	2667.1	2599.8	2632.1			2895.1	
13	2935	2863.7	2884.5	2876.3			3195.3	3163.4
14	3259.9	3320.7	3176.0	3192.4			3508.1	
15	3582.8	3519.0	3467.5				3811.0	3826.0
16	3917.9	3991.5	3748.7	3736.8				
17	4252.2	4242.1						
rms	45		26		23		28	

Table 3. The same as Table 2, but for ^{148}Ce and ^{150}Ce. Parameters in Figure 4.

	^{148}Ce		^{150}Ce			^{148}Ce		^{150}Ce	
I	Th	Exp	Th	Exp	I	Th	Exp	Th	Exp
1	371.6		463.4		12	2330.0	2327.8	1920.0	1918.5
2	236.9	158.8	177.4	97.0	13	2765.3	2751.7	2659.4	2639.1
3	588.7		692.1		14	2915.2	2887.9	2488.6	2465.0
4	442.7	453.5	314.9	305.7	15	3343.5	3326.4	3183.5	3177.7
5	894.5		974		16	3517.2	3464.1	3090.5	3058.2
6	777.8	839.5	580.2	606.4	17	3936.2	3944.2	3740.7	3744.3
7	1284.6	1351.4	1317.3	1385.6	18	4118.1	4065.8	3710.1	3694.2
8	1219.9	1290.3	948.7	982.6	19	4474.6		4290.9	
9	1722.9	1753.6	1717.6	1732.7	20	4701.6	4685.8	4332.6	4367.3
10	1746.0	1790.7	1401.1	1422.6	21	4991.4			
11	2220.6	2224.7	2167.7	2153.6	22	5251.9	5312.0		
rms						44		33	

and ^{146}Ba (Figure 2), we remak that the description of so sharply decreasing (in the beginning) staggering amplitude together with the second staggering region is principally complicated task for the double-well potential bound to the QO

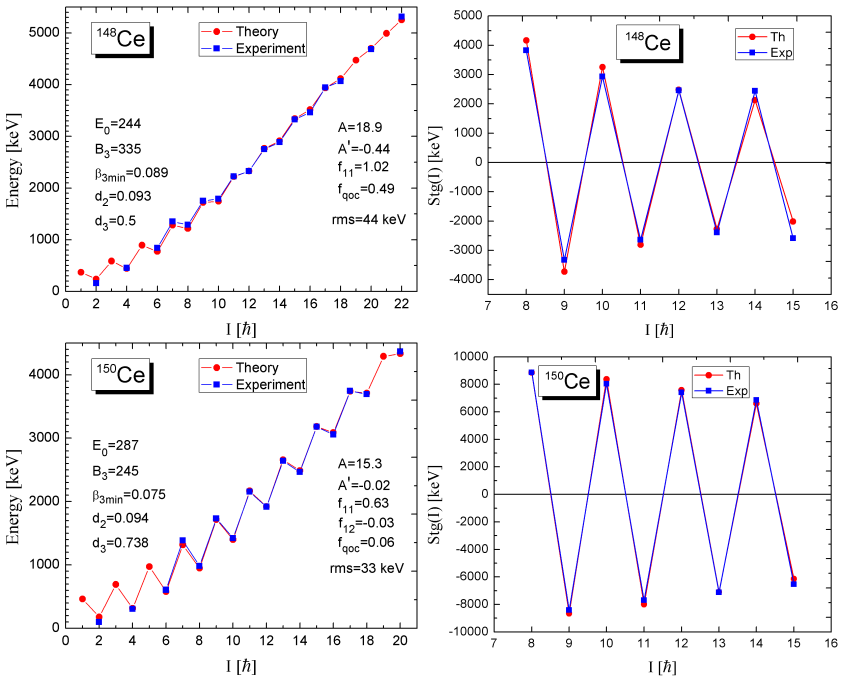

Figure 4. The same as Figure 2, but for ^{148}Ce and ^{150}Ce.

rotor. As a consequence the theoretical staggering amplitude in the higher-spin levels (after the beats) appears much smaller compared to the experimental one. Perhaps a better result could be achieved if one try to fit separately the double-well and the QO rotor parameters in the lower and upper part of the spectrum, respectively. However we leave this refinement for a further work. In ^{144}Ce we get the best rms=23 keV, but it should be fairly remarked that in this nucleus, as well as, in ^{146}Ce the available experimental level-sequence is relatively short and the second staggering region (the beat), though approached, is not reached. In the nuclei ^{148}Ce and ^{150}Ce the staggering amplitudes decrease slowly. Here the double-well performs reasonably well and obviously the QORM contribution in the description is minor (no even sings of the "beat" effect). Actually the staggering patterns in Figure 4 suggest that the octupole mode in ^{148}Ce and ^{150}Ce is rather soft and these two nuclei may need to be described within the CQOM model [5]. Still, we remark that the present model description for both nuclei is quite reasonable. The other circumstance, indicated in Table 1, is the rather different rotation structure of the positive- and negative-parity levels in Ba-Ce spectra, which should be taken into account in the assessment of the quality of the model description. We remark that given this complication, still the model reasonably good reproduces the structure of both sequences. This means that the

parity-splitting effect generated by the double-well potential in the model rather plausibly incorporates the different rotation behaviour of the opposite-parity sequences in the considered Ba-Ce nuclei.

5 Summary

In summary, we have made a phenomenological analysis of the structure of AP spectra in the nuclei of Ba-Ce region (two-parabolas fit) and performed QORM model calculations for the spectra of the nuclei ^{144,146}Ba and ^{144,146,148,150}Ce. The assessment of the obtained (preliminary) description in the context of the revealed specific band-structures in Ba-Ce nuclei confirms the validity of the QORM model concept. The more detailed application of the model in this region as well as in the other regions of quadrupole-octupole collectivity would require the involvement of B(E1), B(E2) and B(E3) transition probabilities in the study. This is the subject of further work.

Acknowledgments

This work has been supported by the Bulgarian National Science Fund under contract No. DFNI-E02/6.

References

[1] J.M. Eisenberg and W. Greiner, *Nuclear Theory: Nuclear Models* (North-Holland, Amsterdam, 1987), third, revised and enlarged edition, Vol. I.

[2] P.A. Butler and W. Nazarewicz, *Rev. Mod. Phys.* **68** (1996) 349.

[3] N. Minkov, S. Drenska, P. Raychev, R. Roussev and D. Bonatsos, *Phys. Rev. C* **63** (2001) 044305.

[4] N. Minkov, P. Yotov, S. Drenska and W. Scheid, *J. Phys. G: Nucl. Part. Phys.* **32** (2006) 497.

[5] N. Minkov, P. Yotov, S. Drenska, W. Scheid, D. Bonatsos, D. Lenis and D. Petrellis, *Phys. Rev. C* **73** (2006) 044315.

[6] N. Minkov, S. Drenska, P. Yotov, S. Lalkovski, D. Bonatsos and W. Scheid, *Phys. Rev. C* **76** (2007) 034324.

[7] N. Minkov, S. Drenska, M. Strecker, W. Scheid and H. Lenske, *Phys. Rev. C* **85** (2012) 034306.

[8] N. Minkov, S. Drenska, K. Drumev, M. Strecker, H. Lenske and W. Scheid, *Phys. Rev. C* **88** (2013) 064310.

[9] N. Minkov, *Rom. J. Phys.* **58**, 1130 (2013).

[10] L.P. Gaffney et al., *Nature* (London) **497** (2013) 199.

[11] B. Bucher et al., *Phys. Rev. Lett.* **116** (2016) 112503.

[12] `http://www.nndc.bnl.gov/ensdf/`.